Journal of Computational Mathematics
Vol.28, No.1, 2010, 87–104.

http://www.global-sci.org/jcm
doi:10.4208/jcm.2009.09-m2935

NUMERICAL IMPLEMENTATION FOR A 2-D THERMAL INHOMOGENEITY THROUGH THE DYNAMICAL PROBE METHOD *

Lei Yi
Institute of mathematics, Fudan University, Shanghai 200433, China
Email: 051018020@fudan.edu.cn
Kyoungsun Kim
Department of Mathematics, Hokkaido University, Sapporo, Japan
Email: kim@math.sci.hokudai.ac.jp
Gen Nakamura
Department of Mathematics, Hokkaido University, Sapporo, Japan
Email: gnaka@math.sci.hokudai.ac.jp

Abstract

In this paper, we present the theory and numerical implementation for a 2-D thermal inhomogeneity through the dynamical probe method. The main idea of the dynamical probe method is to construct an indicator function associated with some probe such that when the probe touch the boundary of the inclusion the indicator function will blow up. From this property, we can get the shape of the inclusion. We will give the numerical reconstruction algorithm to identify the inclusion from the simulated Neumann-to-Dirichlet map.

Mathematics subject classification: 35R30.
Key words: Heat equation, Dynamical probe method, Neumann-to-Dirichlet map.

1. Introduction

Let Ω be a bounded domain in $\mathbb{R}^2$ with C^2 boundary $\partial\Omega$. We consider a heat conductor Ω with an inclusion D such that $\overline{D} \subset \Omega$, $\Omega \setminus \overline{D}$ is connected and the boundary ∂D of D is of class $C^{1,\alpha}$ $(0 < \alpha \leq 1)$. Let the heat conductivity $\gamma(x)$ in Ω be given as follows:

$$\gamma(x) = \begin{cases} 1 & \text{for } x \in \Omega \setminus \overline{D} \\ k & \text{for } x \in D \end{cases}$$

with a positive constant k which is not 1. That is, by using the characteristic function χ_D of D, $\gamma(x)$ is given as $\gamma(x) = 1 + (k-1)\chi_D$.

Here Ω could be a cross section of a heat conductive bar which contains an unknown inclusion with a uniform cross section D. We are concerned with a thermographic nondestructive testing to identify D. This testing is to identify D from the measurements which apply heat flux (sometime called thermal load) to $\partial\Omega$ many times and measure the corresponding temperature on $\partial\Omega$. For more details, the readers can refer to [15], [16] and the references therein. In this paper, we will provide both theoretical and numerical schemes for this testing.

* Received October 16, 2008 / Revised version received March 19, 2009 / Accepted May 7, 2009 / Published online October 26, 2009 /

First of all, we will give some notations which will be used throughout this paper. For a set B, $B \times (T_1, T_2)$ and $B \times (0, T)$ are denoted by $B_{(T_1,T_2)}$ and B_T, respectively. Also, for $p, q \in \mathbb{Z}_+ := \mathbb{N} \cup \{0\}$ or $p = \frac{1}{2}$, $H^p(\Omega), H^p(\partial\Omega)$ and $H^{p,q}(\Omega_T)$ denote the usual Sobolev spaces, where p and q in $H^{p,q}(\Omega_T)$ denote the regularity with respect to x and t, respectively (cf. [12]). Further, for an open set $U \subset \mathbb{R}^3$ with Lipschitz boundary ∂U and $p, q \in \mathbb{Z}_+$, $H^{p,q}(U)$ is defined similar to $H^{p,q}(\Omega_T)$. That is $g \in H^{p,q}(U)$ if and only if there exists $\mathbf{g} \in H^{p,q}(\mathbb{R}^3)$ with $g = \mathbf{g}$ in U. The norm $||g||_{H^{p,q}(U)}$ of g defined by

$$||g||_{H^{p,q}(U)} := \inf \left\{ ||\mathbf{g}||_{H^{p,q}(\mathbb{R}^3)}; \mathbf{g} \in H^{p,q}(\mathbb{R}^3) \text{ and } \mathbf{g}|_U = g \right\}.$$

Moreover, a function $f(x,t)$ is in $L^2((0,T);X)$ if $f(\cdot,t) \in X$ for almost all $t \in (0,T)$ and

$$||f||^2_{L^2((0,T);X)} = \int_0^T ||f(\cdot,t)||^2_X dt < \infty.$$

The forward problem for the thermographic nondestructive testing is to find a unique weak solution $u = u(f) \in H^{1,0}(\Omega_T)$ which satisfies

$$\begin{cases} \mathcal{P}_D u(x,t) := \partial_t u(x,t) - \operatorname{div}_x(\gamma(x)\nabla_x u(x,t)) = 0 \quad \text{in } \Omega_T \\ \partial_\nu u(x,t) = f(x,t) \quad \text{in } \partial\Omega_T, \quad u(x,0) = 0 \quad \text{for } x \in \Omega \end{cases} \tag{1.1}$$

for a given $f \in L^2((0,T);(H^{1/2}(\partial\Omega))^*)$. Namely, by assuming the initial temperature of a heat conductive medium Ω is 0, determine the temperature $u = u(f)$ induced in Ω_T after applying the heat flux f on $\partial\Omega_T$.

By a weak solution $u = u(f) \in H^{1,0}(\Omega_T)$ of Problem (1.1), we mean a function $u = u(f)$ which satisfies

$$\int_{\Omega_T} (-u\partial_t\varphi + \gamma(x)\nabla_x u \cdot \nabla_x \varphi) dx dt = \int_{\partial\Omega_T} f\varphi|_{\partial\Omega_T} d\sigma dt$$

for all

$$\varphi \in W(\Omega_T) := \left\{ v \in H^{1,0}(\Omega_T); \partial_t v \in L^2((0,T);(H^1(\Omega))^*) \right\}$$

with $\varphi(x,T) = 0$ for all $x \in \Omega$.

It is well known that the boundary value problem (1.1) is well posed (see [17]). That is there exists a unique solution $u = u(f) \in H^{1,0}(\Omega_T)$ to (1.1) and $u(f)$ depends continuously on $f \in L^2((0,T);(H^{1/2}(\partial\Omega))^*)$. Based on this, we define the *Neumann-to-Dirichlet map* Λ_D : $L^2((0,T);(H^{1/2}(\partial\Omega))^*) \to L^2((0,T);H^{1/2}(\partial\Omega))$ by $\Lambda_D(f) = u(f)|_{\partial\Omega_T}$.

Now, we take the Neumann-to-Dirichlet map Λ_D as measured data for our nondestructive testing. Then, our inverse problem is to reconstruct the unknown inclusion D from Λ_D.

In [3], authors gave a reconstruction procedure for one space dimensional case. It is an analogue of the probe method which was introduced by Ikehata [7] to identify the shape of unknown inclusion in a stationary heat conductive medium. They gave a theory on how to adapt the probe method for the stationary heat conductive case and provided a reconstruction scheme identifying an inclusion which can depend on time for one space dimensional case. Below, we will refer this kind of dynamical version of the probe method by *dynamical probe method*. Further, Isakov, Kim, and Nakamura [8] extended this argument and established the foundation for dynamical probe method.

Isakov, Kim, and Nakamura gave the proof of probe method for the three dimensional case in [8]. As the proof is quite different for the two space dimensional case, in this work we will

provide not only some numerical results but also the proof of the dynamical probe method for the two space dimensional case.

The rest of this paper is organized as follows. In Sections 2 and 3, we define the indicator function which will be proved to be the right one for the reconstruction of inhomogeneity. In Sections 4 and 5, we give the numerical reconstruction algorithm to identify the inclusion from the simulated Neumann-to-Dirichlet map.

2. Preliminary Results on Dynamical Probe Method

For $(y,s),(y,s') \in (\Omega \setminus \overline{D})_T$ such that $s \neq s'$, let $\Gamma(x,t;y,s)$ and $\Gamma^*(x,t;y,s')$ for $(x,t) \in \Omega_T$ be

$$\Gamma(x,t;y,s) = \begin{cases} \dfrac{1}{4\pi(t-s)} \exp\Big[-\dfrac{|x-y|^2}{4(t-s)} \Big], & t > s, \\ 0, & t \leq s, \end{cases}$$

$$\Gamma^*(x,t;y,s') = \begin{cases} 0, & t \geq s', \\ \dfrac{1}{4\pi(s'-t)} \exp\Big[-\dfrac{|x-y|^2}{4(s'-t)} \Big], & t < s'. \end{cases}$$

Then,

$$\mathcal{P}_\emptyset \Gamma(x,t;y,s) := (\partial_t - \triangle_x)\Gamma(x,t;y,s) = 0 \text{ if } (x,t) \neq (y,s)$$

and

$$\mathcal{P}^*_\emptyset \Gamma^*(x,t;y,s') := (-\partial_t - \triangle_x)\Gamma^*(x,t;y,s') = 0 \text{ if } (x,t) \neq (y,s').$$

By Runge's approximation theorem proved in [3] and the interior regularity estimate (see, e.g., [6]), we have the following result.

Proposition 2.1. *Let $f \in L^2((0,T);(H^{1/2}(\partial\Omega))^*)$. We can select two sequences of functions $\{v^j_{(y,s)}\}$ and $\{\varphi^j_{(y,s')}\}$ in $H^{2,1}(\Omega_{(-\eta,T+\eta)})$ for arbitrary constant $\eta > 0$ such that*

$$\begin{cases} \mathcal{P}_\emptyset v^j_{(y,s)} = 0 & \text{in} \quad \Omega_{(-\eta,T+\eta)}, \\ v^j_{(y,s)}(x,t) = 0 & \text{if} \quad -\eta < t \leq 0, \\ v^j_{(y,s)} \to \Gamma(\cdot,\cdot;y,s) & \text{in} \quad H^{2,1}(U_T) \quad \text{as} \quad j \to \infty, \end{cases} \tag{2.1}$$

and

$$\begin{cases} \mathcal{P}^*_\emptyset \varphi^j_{(y,s')} = 0 & \text{in} \quad \Omega_{(-\eta,T+\eta)}, \\ \varphi^j_{(y,s')}(x,t) = 0 & \text{if} \quad T \leq t < T+\eta, \\ \varphi^j_{(y,s')} \to \Gamma^*(\cdot,\cdot;y,s') & \text{in} \quad H^{2,1}(U_T) \quad \text{as} \quad j \to \infty \end{cases} \tag{2.2}$$

for each open set U_T in $\Omega_{(-\eta,T+\eta)}$ such that $\overline{U}_T \subset \Omega_{(-\eta,T+\eta)}$, $\Omega_{(-\eta,T+\eta)} \setminus \overline{U_T}$ is connected, U_T has a Lipschitz boundary ∂U_T, and $\overline{U}_T$ does not contain (y,s) and (y,s'). We call these functions in sequences $\{v^j_{(y,s)}\}$ and $\{\varphi^j_{(y,s')}\}$ Runge's approximation functions.

We now define the pre-indicator function, which will be used later to define an indicator function which is a mathematical testing machine to identify the unknown inclusion.

Definition 2.2. ([3]) Let $(y,s),(y,s') \in \Omega_T$ be such that $s \neq s'$, and $\{v^j_{(y,s)}\},\{\varphi^j_{(y,s')}\} \subset H^{2,1}(\Omega_{(-\eta,T+\eta)})$ be Runge's approximation functions given by (2.1) and (2.2). Then, we define the pre-indicator function $I(y,s';y,s)$ as follows.

$$I(y,s';y,s) = \lim_{j\to\infty} \int_{\partial\Omega_T} \left(\partial_\nu v^j_{(y,s)}|_{\partial\Omega_T}\ \varphi^j_{(y,s')}|_{\partial\Omega_T} - \Lambda_D(\partial_\nu v^j_{(y,s)}|_{\partial\Omega_T})\ \partial_\nu \varphi^j_{(ys')}|_{\partial\Omega_T} \right) \tag{2.3}$$

whenever the limit exists.

For Runge's approximation functions $\{v^j_{(y,s)}\} \subset H^{2,1}(\Omega_{(-\eta,T+\eta)})$ used in the definition above, let

$$u^j_{(y,s)} := u(\partial_\nu v^j_{(y,s)}|_{\partial\Omega_T}) \text{ and } w^j_{(y,s)} := u^j_{(y,s)} - v^j_{(y,s)}.$$

Then, $w^j_{(y,s)}$ satisfies the following mixed boundary value problem

$$\begin{cases} \mathcal{P}_D w^j_{(y,s)} = (k-1)\mathrm{div}_x(\chi_D \nabla_x v^j_{(y,s)}) & \text{in } \Omega_T, \\ \partial_\nu w^j_{(y,s)} = 0 \quad \text{on } \partial\Omega_T, \quad w^j_{(y,s)}(x,0) = 0 & \text{for } x \in \Omega. \end{cases}$$

Then, for the limit of $w^j_{(y,s)}$, we have the following lemma.

Lemma 2.3. ([3]) *$w^j_{(y,s)}$ has a limit $w_{(y,s)} \in W(\Omega_T)$ satisfying*

$$\begin{cases} \mathcal{P}_D w_{(y,s)} = (k-1)\mathrm{div}_x(\chi_D \nabla_x \Gamma(\cdot,\cdot;y,s)) & \textit{in } \Omega_T, \\ \partial_\nu w_{(y,s)} = 0 \quad \textit{on } \partial\Omega_T, \quad w_{(y,s)}(x,0) = 0 & \textit{for } x \in \Omega. \end{cases}$$

We call $w_{(y,s)}$ the *reflected solution*. From the theorems and propositions proved in [3], we have the following representation formula for the pre-indicator function in terms of the reflected solution.

Theorem 2.4. *For $(y,s),(y,s') \in \Omega_T$ with $s \neq s'$, we have*

$$I(y,s';y,s) = -w_{(y,s)}(y,s') - \int_{\partial\Omega_T} w_{(y,s)}(x,t)\partial_\nu \Gamma^*(x,t;y,s')d\sigma(x)dt.$$

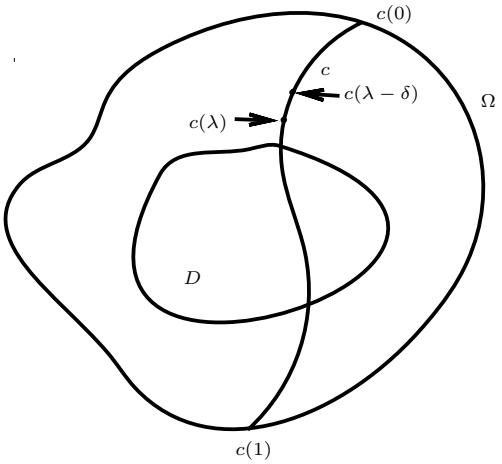

Fig. 2.1. Domains Ω, D, and a curve $C(\lambda)$

We defined the indicator function as follows.

Definition 2.5. *Let $C := \{c(\lambda)\,;\, 0 \le \lambda \le 1\}$ be a non-selfintersecting C^1 curve in $\overline{\Omega}$ which joins $c(0), c(1) \in \partial\Omega$. Then, for each $c(\lambda) \in \Omega_T$ and each fixed $s \in (0,T)$, we define the indicator function $J(c(\lambda), s)$ by*

$$J(c(\lambda), s) := \lim_{\epsilon \to 0} \liminf_{\delta \downarrow 0} |I(c(\lambda - \delta), s + \epsilon^2; c(\lambda - \delta), s)|$$

whenever the limit exists.

By using this indicator function, we can recover D as follows.

Theorem 2.6. *Let C be given as in Definition 2.5 above. Then, for a fixed $s \in (0,T)$, we have the followings.*

(i) If the curve C is in $\Omega \setminus \overline{D}$ except $c(0)$ and $c(1)$, then $J(c(\lambda), s) < \infty$ for all λ, $0 \le \lambda \le 1$.

(ii) Let $C \cap \overline{D} \neq \emptyset$ and λ_s $(0 < \lambda_s < 1)$ be such that $c(\lambda_s) \in \partial D$, $c(\lambda) \in \Omega \setminus \overline{D}$ $(0 < \lambda < \lambda_s)$. Then,

$$\lambda_s = \sup\{\, 0 < \lambda < 1\,;\, J(c(\lambda'), s) < \infty \quad \textit{for any } 0 < \lambda' < \lambda \,\}.$$

Remark 2.7. This result itself is exactly the same as that in [8]. However, for the two dimensional case, the proof needs some changes. The details will be given in next section.

3. Proof of Theorem 2.6

By Theorem 2.4, we can see that the behavior of the indicator function $J(c(\lambda), s)$ is determined by the behavior of the reflected solution $w_{(y,s)}$. When y is not on the boundary of D, $w_{(y,s)}$ is bounded due to the interior regularity estimate. So we only need to know the behavior of $w_{(y,s)}$ when y approaches the boundary of D along the curve.

To begin with let $E(x,t;y,s) := w_{(y,s)}(x,t) + \Gamma(x,t;y,s)$. Then, E is obviously a fundamental solution for the operator $\mathcal{P}_D$. Further, let C be as in Definition 2.5. Now let $P = c(\lambda_0) \in \partial D$ for some λ_0.

Since ∂D is $C^{1,\alpha}$ $(0 < \alpha \le 1)$, there is a $C^{1,\alpha}$ diffeomorphism $\Phi : \mathbb{R}^2 \to \mathbb{R}^2$ which transforms P to the origin O in $\mathbb{R}^2$, $\Phi(D) \subset \mathbb{R}^2_- = \{x = (x_1, x_2) \in \mathbb{R}^2; x_2 < 0\}$, and $D\Phi(P) = I$ (2×2 identity matrix). This Φ is the same as that in the paper. Alessandrini and Di Cristo [1]. For the details we refer the reader to [8].

Let us proceed with our proof. Let Γ_- be the fundamental solution for the operator $\partial_\tau - \mathrm{div}((1 + (k-1)\chi_-)\nabla)$ in $\mathbb{R}^2 \times \mathbb{R}$ with the characteristic function χ_- of the space $\mathbb{R}^2_-$ such that $\Gamma_-(\cdot, \tau; \cdot, \mu) = 0$ for $\tau \le \mu$. Let $\xi = \Phi(x)$ and $\eta = \Phi(y)$. We decompose $w_{(y,s)}$ as follows:

$$\begin{aligned} & w_{(y,s)}(x,t) = E(x,t;y,s) - \Gamma(x,t;y,s) \\ =& \big\{E(x,t;y,s) - \Gamma_-(\Phi(x),t;\Phi(y),s)\big\} + \big\{\Gamma_-(\Phi(x),t;\Phi(y),s) \\ & - \Gamma(\Phi(x),t;\Phi(y),s)\big\} + \big\{\Gamma(\Phi(x),t;\Phi(y),s) - \Gamma(x,t;y,s)\big\}. \end{aligned}$$

Let $\varepsilon > 0$ be given. We take $x = y = y(\delta) = c(\lambda_0 - \delta) \in C \setminus \overline{D}$ so that $y(\delta) \to P\,(\delta \downarrow 0)$. Then, as $\delta \downarrow 0$, $\xi = \eta \to \Phi(P) = O$.

Remark 3.1. When $t > s$, the definition of Γ gives us the fact

$$\Gamma(y,t;y,s) = \frac{1}{4\pi(t-s)}.$$

So, the third parenthesis is zero if we take $x = y$ and $t = s + \varepsilon^2$.

Next, we will estimate the remaining differences in the forthcoming lemmas:

$$\begin{aligned} E(\Phi^{-1}(\xi),t;\Phi^{-1}(\eta),s) - \Gamma_-(\xi,t;\eta,s) \qquad & \text{in Lemma 3.2,} \\ \Gamma_-(\xi,t;\eta,s) - \Gamma(\xi,t;\eta,s) \qquad & \text{in Lemma 3.3.} \end{aligned}$$

To begin with we put $\tilde{E}(\xi,t;\eta,s) := E(\Phi^{-1}(\xi),t;\Phi^{-1}(\eta),s)$. Then, we have the following result.

Lemma 3.2. *If y approaches the boundary of D, then we have*

$$\limsup_{\delta \downarrow 0} (\tilde{E} - \Gamma_-)(\eta, s+\varepsilon^2; \eta, s) = \mathcal{O}(\varepsilon^{\alpha-2}) \quad as \quad \varepsilon \to 0.$$

Proof. Note that $\tilde{E}$ satisfies

$$[\partial_t - \nabla_\xi \cdot ((1+(k-1)\chi_-)M(\xi)\nabla_\xi)]\tilde{E}(\xi,t;\eta,s) = \delta(\xi-\eta)\delta(t-s)$$

in $\mathbb{R}^2 \times \mathbb{R}^1$,where

$$M(\xi) = JJ^T \text{ with } J = \frac{\partial \xi}{\partial x}(\Phi^{-1}(\xi)) \text{ and } \tilde{E}(\xi,t;\eta,s) = 0 \text{ for } t \le s.$$

Then $\tilde{R}(\xi,t;\eta,s) := \tilde{E}(\xi,t;\eta,s) - \Gamma_-(\xi,t;\eta,s)$ satisfies

$$\begin{aligned} &[\partial_t - \nabla_\xi \cdot ((1+(k-1)\chi_-)\nabla_\xi)]\tilde{R}(\xi,t;\eta,s) \\ =&\nabla_\xi \cdot ((1+(k-1)\chi_-)(M-I)\nabla_\xi)\tilde{E}(\xi,t;\eta,s) \end{aligned}$$

in $\mathbb{R}^2 \times \mathbb{R}^1$.

Now, let Γ_-^* be the fundamental solution for $-\partial_t - \mathrm{div}_\xi((1+(k-1)\chi_-)\nabla_\xi)$ such that

$$\Gamma_-^*(\xi,t;z,\tau) = 0 \text{ for } t \ge \tau.$$

Choose a ball $B_r(O)$ with a radius r centered at the origin, so that $\overline{\Phi(\Omega)} \subset B_r(O)$. Then, we have the following representation:

$$\begin{aligned} \tilde{R}(\xi,t;\eta,s) = &\int_s^t \int_{B_r(O)} (1+(k-1)\chi_-)(I-M)\nabla_z \tilde{E}(z,\tau;\eta,s)\cdot \nabla_z \Gamma_-^*(z,\tau;\xi,t)dzd\tau \\ &+ \int_s^t \int_{\partial B_r(O)} (1+(k-1)\chi_-)[\frac{\partial}{\partial \nu_z}\tilde{R}(z,\tau;\eta,s)\Gamma_-^*(z,\tau;\xi,t) \\ &- \tilde{R}(z,\tau;\eta,s)\frac{\partial}{\partial \nu_z}\Gamma_-^*(z,\tau;\xi,t)]d\sigma(z)d\tau. \end{aligned} \tag{3.1}$$

Note that the integration (3.1) is finite by the choice of $B_r(O)$. From the known bounds of fundamental solutions of parabolic equations ([13]), we get

$$|\nabla_z \tilde{E}(z,\tau;\eta,s)| \le c_1(\tau-s)^{-\frac{3}{2}} \exp\Big(-\frac{|z-\eta|^2}{c_2(\tau-s)}\Big), \tag{3.2}$$

$$|\nabla_z \Gamma_-^*(z,\tau;\xi,t)| \le c_3(t-\tau)^{-\frac{3}{2}} \exp\Big(-\frac{|z-\xi|^2}{c_4(t-\tau)}\Big) \tag{3.3}$$

for some positive constants c_i, $1 \le i \le 4$. To proceed further, we use the estimate

$$|M(z) - I| \le c_5 |z|^\alpha \quad (|z| < r)$$

for some constant $c_5 > 0$, because ∂D is $C^{1,\alpha}$. From now on, we use c for some generic constants which do not depend on ε and they do not need to be same. By using the Fatou lemma, the $\limsup_{\delta \downarrow 0}$ of the absolute value of the integration (**??**) can be bounded from above by a constant multiple of the following:

$$\int_s^{s+\varepsilon^2} \int_{|z|<r} |z|^\alpha |\nabla_z \tilde{E}(z,\tau;O,s)||\nabla_z \Gamma_-^*(z,\tau;O,s+\varepsilon^2)| dz d\tau =: F.$$

From the inequalities (3.2)-(3.3), we have

$$\begin{aligned} F &\le c \int_s^{s+\varepsilon^2} \int_{|z|<r} \frac{|z|^\alpha}{(\tau-s)^{3/2}(s+\varepsilon^2-\tau)^{3/2}} \exp\left(-\frac{|z|^2}{c(\tau-s)} - \frac{|z|^2}{c(s+\varepsilon^2-\tau)}\right) dz d\tau \\ &= c\varepsilon^{\alpha-2} \int_0^1 \int_{|\zeta|<r\varepsilon^{-1}} |\zeta|^\alpha (\mu(1-\mu))^{-\frac{3}{2}} \exp\left(-\frac{|\zeta|^2}{c\mu} - \frac{|\zeta|^2}{c(1-\mu)}\right) d\zeta d\mu \\ &\le c\varepsilon^{\alpha-2} \int_0^1 \int_{\mathbb{R}^2} |\zeta|^\alpha (\mu(1-\mu))^{-\frac{3}{2}} \exp\left(-\frac{|\zeta|^2}{c\mu(1-\mu)}\right) d\zeta d\mu. \end{aligned}$$

Using polar coordinates, we have

$$\begin{aligned} F &\le c\varepsilon^{\alpha-2} \int_0^1 \int_0^\infty r^{\alpha+1} (\mu(1-\mu))^{-\frac{3}{2}} \exp\Big[-\frac{r^2}{c\mu(1-\mu)}\Big] dr d\mu \\ &\le c\varepsilon^{\alpha-2} \int_0^1 [\mu(1-\mu)]^{\frac{\alpha-1}{2}} d\mu \int_0^\infty s^{\alpha+1} e^{-s^2} ds \le c\varepsilon^{\alpha-2}. \end{aligned}$$

Therefore we have

$$\limsup_{\delta \downarrow 0} |\tilde{R}(\eta, s+\varepsilon^2; \eta, s)| \le c\varepsilon^{\alpha-2},$$

which is the desired result. □

Now fix (η, s) and put

$$W(\xi, t) := \Gamma_-(\xi, t; \eta, s) - \Gamma(\xi, t; \eta, s).$$

Let $W^\pm(\xi, t)$ for $\pm\xi_2 > 0$. Then, we have the following lemma.

Lemma 3.3. *If y approaches the boundary of D, then there is a constant C which does not depend on ε such that*

$$\lim_{\delta \downarrow 0} W^+(\xi, s+\varepsilon^2) = C\varepsilon^{-2} \quad as \quad \varepsilon \to 0.$$

Proof. Since Γ and Γ_- satisfy the following equations

$$\begin{cases} \partial_t \Gamma_-(\xi,t;\eta,s) - \nabla_\xi \cdot (1 + (k-1)\chi_-)\nabla_\xi \Gamma_-(\xi,t;\eta,s) = \delta(\xi-\eta)\delta(t-s) \\ \partial_t \Gamma(\xi,t;\eta,s) - \triangle_\xi \Gamma(\xi,t;\eta,s) = \delta(\xi-\eta)\delta(t-s) \end{cases}$$

in $\mathbb{R}^2 \times \mathbb{R}^1$, we can see that W satisfies

$$\partial_t W(\xi,t) - \nabla_\xi \cdot \big((1 + (k-1)\chi_-)\nabla_\xi W(\xi,t)\big) = (k-1)\nabla_\xi \cdot \big(\chi_- \nabla_\xi \Gamma(\xi,t;\eta,s)\big).$$

As in [8], by using the Laplace transform and the Fourier transform, we get the representation of $W^+(\xi,t)$ as follows:

$$W^+(\xi,t)=\frac{\sqrt{k-1}}{8\pi^2}\int_0^1\frac{\sqrt{r}+i\sqrt{k(1-r)}}{\sqrt{r}(\sqrt{r}-i\sqrt{k(1-r)})}F(r)dr,$$

where

$$\begin{aligned}F(r)=\int_{\mathbb{R}}|\zeta|e^{i(\xi_1-\eta_1)\zeta}\Big[&\exp\{-(t-s)\zeta^2(kr-r+1)-i(\xi_2+\eta_2)\sqrt{k-1}|\zeta|\sqrt{r}\}\\&+\exp\{-(t-s)\zeta^2(kr-r+1)+i(\xi_2+\eta_2)\sqrt{k-1}|\zeta|\sqrt{r}\}\Big]d\zeta.\end{aligned}$$

Now let $\delta\downarrow 0$ and set $t=s+\varepsilon^2$. Then, $\xi=\eta\to O$ and $(t-s)(kr-r+1)>0$. Consequently,

$$\begin{aligned}\lim_{\delta\downarrow 0}F(r)&=2\int_{\mathbb{R}}|\zeta|\exp[-\varepsilon^2(kr-r+1)\zeta^2]d\zeta\\&=4\int_0^\infty\zeta\exp[-\varepsilon^2(kr-r+1)\zeta^2]d\zeta=\frac{2\varepsilon^{-2}}{kr-r+1}.\end{aligned}$$

Therefore we have

$$\begin{aligned}&\lim_{\delta\downarrow 0}W^+(\xi,s+\varepsilon^2)\\=&\frac{\sqrt{k-1}}{4\pi^2}\varepsilon^{-2}\int_0^1\frac{\sqrt{r}+i\sqrt{k(1-r)}}{\sqrt{r}(\sqrt{r}-i\sqrt{k(1-r)})}\frac{1}{kr-r+1}dr=\frac{\sqrt{k-1}}{4\pi^2}\varepsilon^{-2}H.\end{aligned}$$

In order to estimate $|H|$ from above and below, we note the following estimates:

$$\left|\frac{\sqrt{r}+i\sqrt{k(1-r)}}{\sqrt{r}-i\sqrt{k(1-r)}}\right|=1,\quad ,1\le kr-r+1\le k,\ 1\le r+k(1-r)\le k.$$

Then we have

$$|H|\le\int_0^1\frac{1}{\sqrt{r}}dr=2<\infty,$$

and the imaginary part of H, $\Im H$, becomes

$$\Im H=2\sqrt{k}\int_0^1\frac{\sqrt{1-r}}{(kr-r+1)(r+k(1-r))}dr\ge\frac{2}{k\sqrt{k}}\int_0^1\sqrt{1-r}dr=\frac{4}{3k\sqrt{k}}>0.$$

This completes the proof. □

By combining results in this section, we conclude that

$$\liminf_{\delta\downarrow 0}|w_{(y(\delta),s)}(y(\delta),s+\varepsilon^2)|\ge C\varepsilon^{-2},$$

as $\varepsilon\to 0$ for some positive constant C independent of ε. That is, the reflected solution blows up as the point approaches the boundary of the inhomogeneity. Furthermore, to get the blow up property we only use the perturbation in time.

4. Runge's Approximation Functions in Dynamical Probe Method

In this section, we present the mathematic framework which is necessary for the numerical realization of Runge's approximation. Let

$$v^g(x,t) = \mathcal{H}(g)(x,t) = \int_0^t \int_{\partial\Omega} \Gamma(x,t;\xi,\tau) g(\xi,\tau) d\sigma(\xi) d\tau, \tag{4.1}$$

with a density function $g(\xi,\tau) \in L^2(\partial\Omega_T)$. Then it is easy to verify $\mathcal{H}(g)$ satisfies

$$\mathcal{P}_\emptyset \mathcal{H}(g)(x,t) = 0, \ (x,t) \in \Omega_T.$$

Let U be as in the Proposition 2.1 and V be similar to U such that $\overline{U} \subset V$. For $(y,s) \in (\Omega \backslash \overline{V})_T$, we consider the integral equation

$$\int_0^t \int_{\partial\Omega} \Gamma(x,t;\xi,\tau) g(\xi,\tau) \mathrm{d}\sigma(\xi) \mathrm{d}\tau \approx \Gamma(x,t;y,s) \quad \text{for} \quad (x,t) \in \partial V_{T+\eta}, \tag{4.2}$$

where the notation $\approx$ means that the right hand side of (4.2) is approximately equal to the left hand side of (4.2). We call this equation Volterra-Fredholm integral equation.

For the existence $g(\xi,\tau)$ in (4.2), we have following theorem.

Theorem 4.1. *For each bounded domain $V \subset \Omega$ with C^2 boundary, the operator $H : L^2(\partial\Omega_T) \to L^2(\partial V_T)$ defined by* (4.1) *has dense range in $L^2(\partial V_T)$*

The proof of this theorem was given in [4] based on the argument provided by the third author of the present paper. Since [4] is a thesis, which is not easy to access, we give the proof for reader's convenience.

Proof. Let $V \subset \Omega$, and $V_T \subset \Omega_{(-\infty,T)}$ be a approximate domain with C^2 lateral boundary ∂V_T. The operator S is same with operator $\mathcal{H}$ in ∂V_T.

Since $L^2(\partial V_T) = \overline{R(S)} \oplus N(S^*)$ with $N(S^*) = \{\psi \in L^2(\partial V_T; S^*\psi = 0\}$, it is sufficient to prove $\Gamma(x,t;\xi,\tau) \in N(S^*)^\perp$. First of all, we note that S^* is given by

$$\Psi(\xi,\tau) := S^*(\psi)(\xi,\tau) = \int_{\partial V_T} \Gamma(x,t;\xi,\tau)\psi(x,t)\mathrm{d}\sigma(x)\mathrm{d}t.$$

Let $\psi = \psi(x,t) \in N(S^*)$ be such that $\psi \in C^0(\overline{\partial V_T})$ and $\psi\big|_{t=0} = 0$. Note that such ψ is dense in $N(S^*)$ and $S^* : L^2(\partial V_T) \to L^2(\Omega_{(-\infty,T)})$ is bounded operator. We continuously extend ψ to $t < 0$ and use the same ψ for the extended ψ. (Of course for this, we need to extend V_T to $t < 0$ without destroying the regularity of its lateral boundary). Then, we have

$$\begin{cases} \mathcal{P}_\phi^* \Psi = 0 \quad \text{in } (\mathbb{R}^2 \setminus \overline{\Omega})_{(-\infty,T)}, \\ \Psi = 0 \quad \text{on } \partial\Omega_{(-\infty,T)}, \quad \Psi\big|_{\tau=T} = 0 \quad \text{on } \mathbb{R}^2 \setminus \overline{\Omega}. \end{cases}$$

For $t > \tau, x \neq \xi$

$$\begin{aligned} \Gamma(x,t;\xi,\tau) =& \frac{1}{4\pi(t-\tau)} \exp\left(-\frac{|x-\xi|^2}{4(t-\tau)}\right) \\ &\leq \pi^{-1}|x-\xi|^{-2} \left(\frac{|x-\xi|^2}{4(t-\tau)}\right)^\alpha (1-\alpha)^{1-\alpha} e^{-(1-\alpha)} \\ &\leq M(t-\tau)^{-\alpha}|x-\xi|^{-2+2\alpha} \end{aligned}$$

for some $M > 0$ with $0 < \alpha < 1$(cf. (9.15) in [10]). Similarly

$$|\nabla_\xi \Gamma(x,t;\xi,\tau)| \le M^{'}(t-\tau)^{-\beta}|x-\xi|^{-2+2\beta}$$

for some $M^{'} > 0$ with $0 < \beta < 2$. Take $0 < \alpha < \frac{1}{2} < \beta < 1, \alpha + \beta < 1$, we have

$$|\Psi(\xi,\tau)| \le M||\psi||_{L^\infty(\partial V_T)}\big(\mathrm{dist}(\partial V_T, \partial\Omega_T)\big)^{-2+2\alpha}|\Omega|(1-\alpha)^{-1}(T-\tau)^{1-\alpha},$$

which gives $\mathcal{O}(|\tau|^{-\alpha})(s \to -\infty)$.

Therefore, summing up all the behaviors, we have

$$\Psi(\xi,\tau) = \begin{cases} \mathcal{O}((T-\tau)^{1-\alpha}) \ (\tau \to T);\ \mathcal{O}((T-\tau)^{1-\alpha})\mathcal{O}(|\xi|^{-2+2\alpha}) \ (\tau \to T, |\xi| \gg 1); \\ \mathcal{O}(|\tau|^{-\alpha})(\tau \to -\infty);\ \mathcal{O}((\tau)^{-\alpha})\ \mathcal{O}(|\xi|^{-2+2\alpha}) \ (\tau \to -\infty, |\xi| \gg 1). \end{cases}$$

Similarly, we have the same estimate for $\nabla_\xi \Psi$ by replacing α by β. Now, let $K_R := (\mathbb{R}^2 \backslash \overline{\Omega}) \cap B_R$ with $B_R := \{|\xi| < R\}$ for large $R > 0$. Then

$$0 = \int_{K_R(-\infty,T)} \Psi \mathcal{P}_\phi^* \Psi \mathrm{d}\xi\mathrm{d}\tau = \int_{K_R(-\infty,T)} |\nabla_\xi \Psi|^2 \mathrm{d}\xi\mathrm{d}\tau - \int_{\partial B_R(-\infty,T)} \Psi \partial_\nu \Psi \mathrm{d}\sigma(\xi)\mathrm{d}\tau$$

because

$$||\Psi(\cdot,T)^2||_{L^2(K_R)} = ||\Psi(\cdot,-\infty)^2||_{L^2(K_R)} = 0$$

and

$$\Psi = 0 \quad \text{on} \quad \Omega_{(-\infty,T)}.$$

Therefore

$$\lim_{R\to\infty} \int_{K_R} |\nabla_\xi \Psi|^2 \mathrm{d}\xi\mathrm{d}\tau = 0. \tag{4.3}$$

Observe that

$$\begin{aligned} &\left| \int_{\partial B_R(-\infty,T)} \Psi \partial_\nu \Psi \mathrm{d}\sigma(\xi)\mathrm{d}\tau \right| \\ \le & L\left(\int_{\frac{T}{2}}^{T} (T-\tau)^{2-(\alpha+\beta)}\mathrm{d}\tau + \int_{-\infty}^{\frac{T}{2}} |\tau|^{\frac{1}{2}-\beta}\mathrm{d}\tau \right) \int_S R^{-3+2(\alpha+\beta)}\mathrm{d}S \\ = & L^{'} R^{-3+2(\alpha+\beta)}|S| \to 0 (R \to \infty). \end{aligned}$$

From (4.3) and $\Psi = 0$ on $\Omega_{(-\infty,T)}$, we obtain

$$\Psi = 0 \ \text{ in } \ (\mathbb{R}^2 \backslash \overline{\Omega})_{(-\infty,T)}.$$

Therefore, by the unique continuation,

$$\Psi(\xi,\tau) = \int_{\partial V_T} \Gamma(x,t;\xi,\tau)\psi(x,t)\mathrm{d}\sigma(x)\mathrm{d}t = 0$$

for $\psi \in N(S^*)$. This completes the proof of the theorem □

By Theorem 4.1, there exist a density function $g^j(\xi,\tau) \in L^2(\partial\Omega_{T+\eta})$ satisfying

$$g^j(\xi,\tau) = \inf\big\{ g(\xi,\tau) : ||\mathcal{H}(g)(\cdot) - \Gamma(\cdot;y,s)||_{L^2(\partial V_{T+\eta})} \le \varepsilon(j) \big\}, \tag{4.4}$$

where $\lim_{j\to\infty}\varepsilon(j)=0$. Thus, together with the interior regularity estimate, we have Runge's approximation v^j in an approximated domain U_T for $\mathcal{P}_\phi$.

On the other hand, it is obvious that

$$\Gamma^*(x,t;y,s')=\Gamma(x,T-t;y,T-s'). \tag{4.5}$$

So, we can get

$$\varphi^j_{(y,s')}(x,t)=v^j_{(y,T-s')}(x,T-t). \tag{4.6}$$

The numerical realization of Runge's approximation φ^j for $\mathcal{P}^*_\phi$ in the same approximated domain can be given by v^j, if we observe (4.5) due to (4.6).

5. Numerical Implementation of Dynamical Probe Method

Let $\xi_j\in\partial\Omega, j=1,\cdots,m$, $x_i\in\partial\Omega, i=1,\cdots,m$ and $t_n=n(T+\eta)/N$, $n=1,\ldots,N$. Also, let $g(\xi_j,\tau)=\sum_{n=1}^N c_{jn}\chi_n(t)$, where $\chi_n(t)$ is the characteristic function of $(t_{n-1},t_n]$. We approximate $g(\xi,\tau)\mathrm{d}\sigma\mathrm{d}\tau$ in (4.2) along $\partial\Omega$ between ξ_j and ξ_{j+1} by $g(\xi_j,\tau)l_{jj}\mathrm{d}\tau$, where l_{jj} is the distance between ξ_j and ξ_{j+1}. Then, we have

$$\mathbf{Ac}=\mathbf{b} \tag{5.1}$$

with $\mathbf{A}=(\mathbf{A}_{i,j})_{mN\times mN}$, $\mathbf{c}=(\mathbf{c}_j)_{mN\times 1}$ and $\mathbf{b}=(\mathbf{b}_i)_{mN\times 1}$ given by

$$\mathbf{A}_{i,j}=\begin{pmatrix}\Delta_1^{i,j} & 0 & 0 & \cdots & 0\\ \Delta_2^{i,j} & \Delta_1^{i,j} & 0 & \cdots & 0\\ \Delta_3^{i,j} & \Delta_2^{i,j} & \Delta_1^{i,j} & \cdots & 0\\ \vdots & \ddots & \ddots & \ddots & \vdots\\ \Delta_N^{i,j} & \cdots & \Delta_3^{i,j} & \Delta_2^{i,j} & \Delta_1^{i,j}\end{pmatrix}$$

$$\mathbf{c}_j=(c_{j1},c_{j2},\cdots,c_{jN})^T\quad \mathbf{b}_i=(b_{i1},b_{i2},\cdots,b_{iN})^T,$$

where

$$\Delta_n^{i,j}=\int_0^{t_1}\Gamma(x_i,t_n;\xi_j,\tau)l_{jj}\mathrm{d}\tau,$$

which can be calculated using the Gauss-Legendre formula, and $b_{in}=\Gamma(x_i,t_n;y,s)$. The linear system (5.1) can be solved using Hansen's Regularization Tools [5].

Once $g(\xi,\tau)$ is known, we can calculate $v_{(y,s)}(x,t)|_{\partial\Omega_T}$ by using the formula.

$$v_{(y,s)}(x,t)=\int_0^t\int_{\partial\Omega}\Gamma(x,t;\xi,\tau)g(\xi,\tau)\mathrm{d}\sigma(\xi)\mathrm{d}\tau\quad\text{for}\quad(x,t)\in\partial\Omega_T. \tag{5.2}$$

On the other hand, we can also calculate $\partial_\nu v_{(y,s)}(x,t)|_{\partial\Omega_T}$ by using the following jump formula

$$\partial_\nu v_{(y,s)}(x,t)=\frac{1}{2}g(x,t)+\int_0^t\int_{\partial\Omega}\frac{\partial\Gamma(x,t;\xi,\tau)}{\partial\nu}g(\xi,\tau)d\sigma(\xi)d\tau\quad\text{for}\quad(x,t)\in\partial\Omega_T. \tag{5.3}$$

Let Ω be an open disk with radius 1 and center $(0,0)$. An approximate domain $V_{T+\eta}$ defined via V with the boundary ∂V is given as the union of

$$\left\{x=(x_1,x_2):x_2=ax_1^6+bx_1^4+cx_1^2+d,\ |x_1|\le x_1^*,\ x_2>0\right\}$$

and

$$\big\{x=(x_1,x_2): x_1^2+x_2^2=r,\ 0<x_1^*\le|x_1|\le 1,\ x_2>0 \quad \text{or} \quad |x_1|\le 1, x_2\le 0\big\}.$$

This V was used in [2] for the numerical testing of the probe method for the inverse scattering problem. We took the parameters a, b, c, d appropriately so that the C^2 smoothness of ∂V is satisfied.

Let $g_\theta(\xi,\tau)$ be a solution of Eq. (4.2) for $\partial V_{T+\eta}(\theta)$ and rotate $V(0)$ to $V(\theta)$ with $\theta\in(0,2\pi]$. Then, it is easy to see that

$$\partial V(\theta)=\mathbf{M}(\theta)\partial V(0)$$

(see Figs. 5.1 and 5.2), where $M(\theta)$ is an orthogonal matrix

$$\mathbf{M}(\theta)=\begin{pmatrix}\cos(\theta) & -\sin(\theta)\\ \sin(\theta) & \cos(\theta)\end{pmatrix}.$$

By the definition of $g_\theta(\xi,\tau)$, we have

$$\int_0^t\int_{\partial\Omega}\Gamma(x^0,t;\xi,\tau)g_0(\xi,\tau)\mathrm{d}\sigma(\xi)\mathrm{d}\tau\approx\Gamma(x^0,t;y^0,s) \qquad x^0\in\partial V(0), \quad (5.4)$$

$$\int_0^t\int_{\partial\Omega}\Gamma(\mathbf{M}(\theta)x^0,t;\xi,\tau)g_\theta(\xi,\tau)\mathrm{d}\sigma(\xi)\mathrm{d}\tau\approx\Gamma(\mathbf{M}(\theta)x^0,t;\mathbf{M}(\theta)y^0,s) \quad x^0\in\partial V(0). \quad (5.5)$$

By using the facts that

$$|\mathbf{M}(\theta)x^0-\xi|=|x^0-(\mathbf{M}(\theta))^{-1}\xi|, \quad |\mathbf{M}(\theta)x^0-\mathbf{M}(\theta)y^0|=|x^0-y^0|$$

and the definition of Γ, the right hand side of Eq. (5.5) becomes $\Gamma(x^0,t;y^0,s)$, which is same as the right hand side of Eq. (5.4), and the left hand side of Eq. (5.5) becomes

$$\int_0^t\int_{\partial\Omega}\Gamma(x^0,t;(\mathbf{M}(\theta))^{-1}\xi,\tau)\ \ g_\theta(\xi,\tau)\mathrm{d}\sigma(\xi)\mathrm{d}\tau.$$

Also, since Ω is axis-symmetric, the left hand side of Eq. (5.4) becomes

$$\int_0^t\int_{\partial\Omega}\Gamma(x^0,t;(\mathbf{M}(\theta))^{-1}\xi,\tau)g_0((\mathbf{M}(\theta))^{-1}\xi,\tau)\mathrm{d}\sigma(\xi)\mathrm{d}\tau.$$

Hence, the minimum norm solution $g_\theta(\xi,\tau)$ corresponding to domain $\partial V_{T+\eta}(\theta)$ is

$$g_\theta(\xi,\tau)=g_0((\mathbf{M}(\theta))^{-1}\xi,\tau)$$

This property is useful for us to reduce the computational time.

Now we give the algorithm as follows:

1. For given (y,s) and (y,s'), we construct the approximate domain $V_{T+\eta}$ satisfying the conditions: $\overline{D}\subset\subset V$ and $(y,s),(y,s')\in\Omega_T\setminus\overline{V_T}$.
2. We calculate g by solving the integral equation (4.2) with the Hansen regularization tools.

3. Compute $v_{(y,s)}(x,t)|_{\partial\Omega_T}$ and $\partial_\nu v_{(y,s)}(x,t)|_{\partial\Omega_T}$ by using (5.2) and (5.3), respectively. Based on equation (4.6), we compute $\varphi_{(y,s)}(x,t)|_{\partial\Omega_T}$ and $\partial_\nu \varphi_{(y,s)}(x,t)|_{\partial\Omega_T}$.
4. Simulate $\Lambda_D(\partial_\nu v_{(y,s)}(x,t)|_{\partial\Omega_T})$, using the finite element method.
5. Calculate indicator function (2.3) and choose the suitable cutoff constant C_θ to determine the boundary of inclusion.

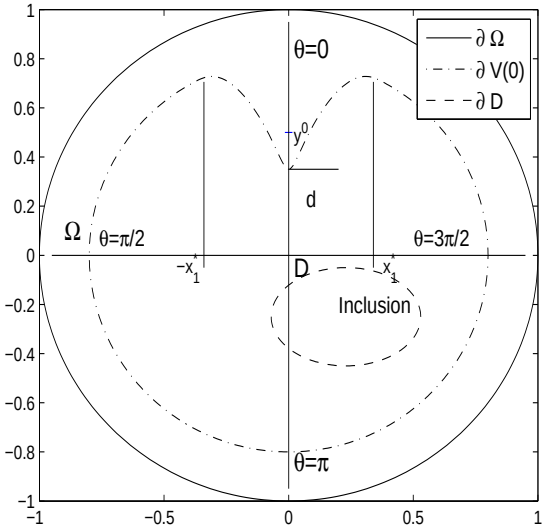

Fig. 5.1. Approximated domain $V(0)$

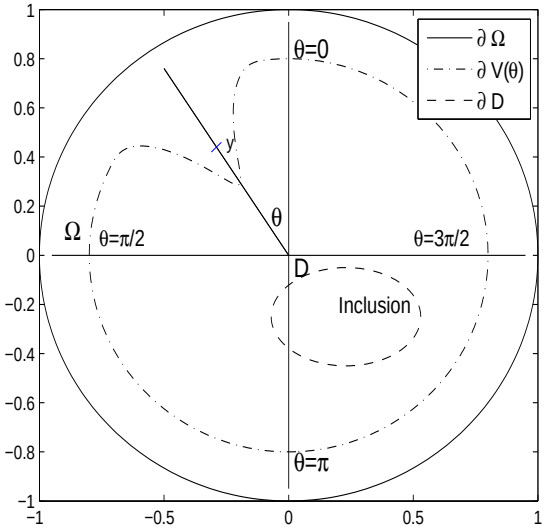

Fig. 5.2. Approximated domain $V(\theta)$ rotating from $V(0)$

Through the analysis of numerical results, we give a rule to choose the cutoff constant C_θ as following:

(1) Obviously, $|I|$ is different due to the different distances between the boundary of inclusion D and Ω. Comparing the value of $|I|$ for $\theta = 0$ and $\theta = \pi/2$ in Table 5.1, we find that the ratio of $|I|$ for $\theta = 0$ to $|I|$ for $\theta = \pi/2$ is about 1, which is approximately the ratio of radius in the two directions for the circle case, and in Table 5.2, we also find that the ratio of $|I|$ for $\theta = 0$ to $|I|$ for $\theta = \pi/2$ is 0.66, which is approximate to the ratio of radius in the two directions for the ellipse case. So C_θ is related to this growth rate, and we define this rate as $k(\theta)$:

$$k(\theta) = \text{AVERAGE}\left(\frac{\text{Indicator}(i, \theta = 0)}{\text{Indicator}(i, \theta)}\right). \tag{5.6}$$

(2) On the other hand, we find the change of $|I|$ is larger than that of $|y|$. If we choose C_θ as constant, the fluctuation of $|I|$ can not reflect the change of $|y|$, it will lose much information, which is called "reduction effect". For this effect, we define $h(\theta)$ as following:

$$h(\theta) = \frac{\sum \text{Indicator}(i, \theta = 0)}{\sum \text{Indicator}(i, \theta)}. \tag{5.7}$$

Based on the above arguments, we define C_θ as

$$C_\theta = C_0 * k(\theta) * h(\theta), \tag{5.8}$$

where C_0 is the value of C_θ when $\theta = 0$.

Now, we will give some examples to test our algorithm. Firstly, we take the parameters as following:

$$m = 34,\ N = 12,\ T = 1,\ \eta = 0.1,\ d = |y| - 0.05,\ s = 0.3,\ s' = 0.5,\ k = 3.$$

Example 1. We consider inclusion with boundary

$$\partial D = \big\{x = (x_1, x_2) = (0.4\cos t, 0.4\sin t), t \in [0, 2\pi]\big\}.$$

We list the values of $|I(y, s'; y, s)|$ in table 5.1.

Table 5.1: Behavior of indicator function as y approaches the boundary

$\|y\|$	$\theta = 0$	$\theta = \pi/2$
0.70	0.4236	0.4490
0.68	0.5689	0.6034
0.66	0.7797	0.8265
0.64	1.0826	1.1455
0.62	1.5118	1.5960
0.60	2.1106	2.2221
0.58	2.9378	3.0843
0.56	4.0594	4.2499
0.54	5.5678	5.8132
0.52	7.5624	7.8757
0.50	10.1941	10.5907
0.48	13.5732	14.0698
0.46	17.9467	18.5638

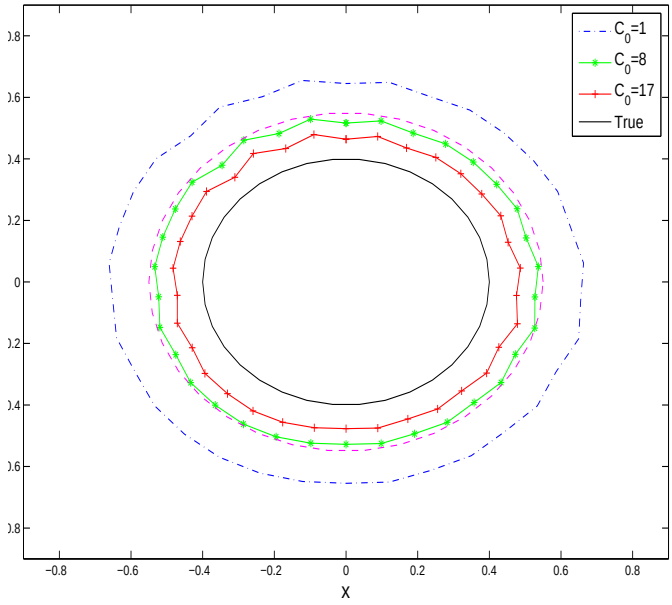

Fig. 5.3. Reconstruction of D for Example 1

If we take the different cutoff constant $C = 1, 8, 17$, we have Figure 5.3.

Example 2. We consider the inclusion with boundary

$$\partial D = \{x = (x_1, x_2) = (0.5\cos t, 0.3\sin t), t \in [0, 2\pi]\}$$

We list the values of $|I(y, s'; y, s)|$ in Table 5.2.

When we take cutoff constant $C_0 = 1, 10, 40$, we have Figure 5.4.

Figures 5.3 and 5.4 show the numerical results for reconstructing the boundary of inclusion with different shapes. The first example is about circular inclusion. We can get the approximate domain of inclusion when $C_0 = 1, 8, 17$, shown in Figure 5.3. The pink line (a circle with radius 0.55) is approximation of green line in Figure 5.3. The second example is about elliptic inclusion. We can also get the approximate domain of inclusion when $C_0 = 1, 10, 40$, shown in Figure 5.4. The pink line (a ellipse with semi-major axis 0.6 and semi-minor axis 0.5) is approximation of green line in Figure 5.4. The numerical results show our algorithm is successful in identifying the shape of unknown inclusion. But in practice, we can not know the center of unknown inclusion. In order to test the effect of our algorithm for general cases, we take the following example. Clearly, if we can estimate the center of the inclusion, the non-center case can be considered as same as the center case.

Example 3. We consider the heart-shaped inclusion with boundary

$$\partial D = \left\{x = (0.1(2 + \cos(t)^5)\cos(t), 0.1(2 + \cos(t)^5)\sin(t)), t \in [0, 2\pi]\right\}$$

with the center $(0.5, 0.2)$, and Ω is a circle with radius 1.5. We list the values of $|I(y, s'; y, s)|$ in Table 5.3.

If we take the different cutoff constant $C = 0.7, 3, 8$, we have Figure 5.5.

Table 5.2: Behavior of indicator function as y approaches the boundary

$\|y\|$	$\theta = 0$	$\theta = \pi/2$
0.70	0.4472	0.6430
0.68	0.6069	0.8979
0.65	0.9942	1.5124
0.62	1.6557	2.5507
0.60	2.3199	3.5840
0.58	3.2333	4.9949
0.56	4.4619	6.8793
0.54	6.0968	9.3706
0.52	8.2332	12.6063
0.50	11.0098	16.7892
0.48	14.5606	22.1117
0.46	19.0720	28.8440
0.44	24.6900	37.1925
0.42	31.7241	47.6038
0.40	40.4213	60.4244

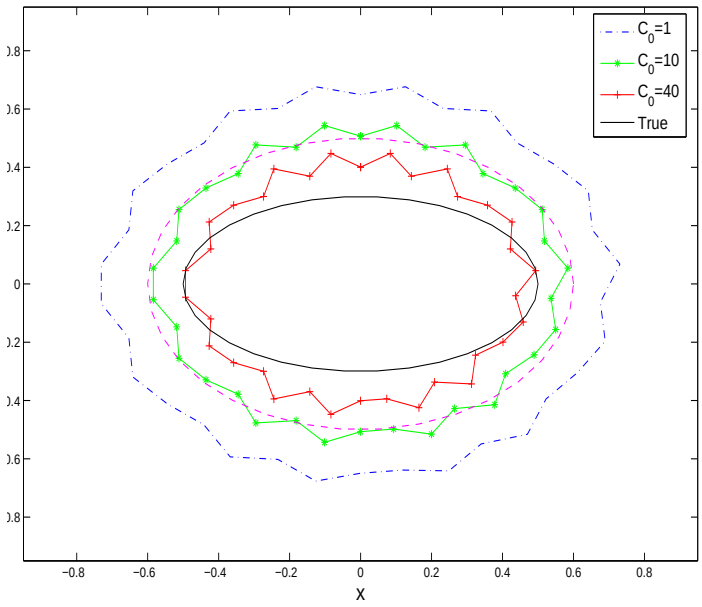

Fig. 5.4. Reconstruction of D for Example 2

In Figure 5.5, we get the reconstruction of heart-shaped inclusion. In Table 5.3, we clearly find the values of indicator function grow quickly in the side where inclusion is close to the boundary of Ω. While in the other side, the values of indicator function grow so slowly that we can not reconstruct the boundary, which can be estimated using the reconstructed boundary, shown in pink line. Especially, base on the approximate domain, we can estimate the center of the inclusion, which is close to the center of inclusion shown in Figure 5.5.

Table 5.3: Behavior of indicator function as y approaches the boundary

$\|y\|$	θ_1	θ_2
1.30	0.0099	0.0087
1.28	0.0099	0.0102
1.26	0.0099	0.0122
1.24	0.0099	0.0149
1.22	0.0099	0.0186
1.20	0.0099	0.0244
1.18	0.0099	0.0342
1.16	0.0099	0.0533
1.14	0.0099	0.0935
1.12	0.0099	0.1819
1.10	0.0099	0.3768
1.08	0.0099	0.8029
1.06	0.0099	1.7077
1.04	0.0100	3.5778
1.02	0.0100	7.2855

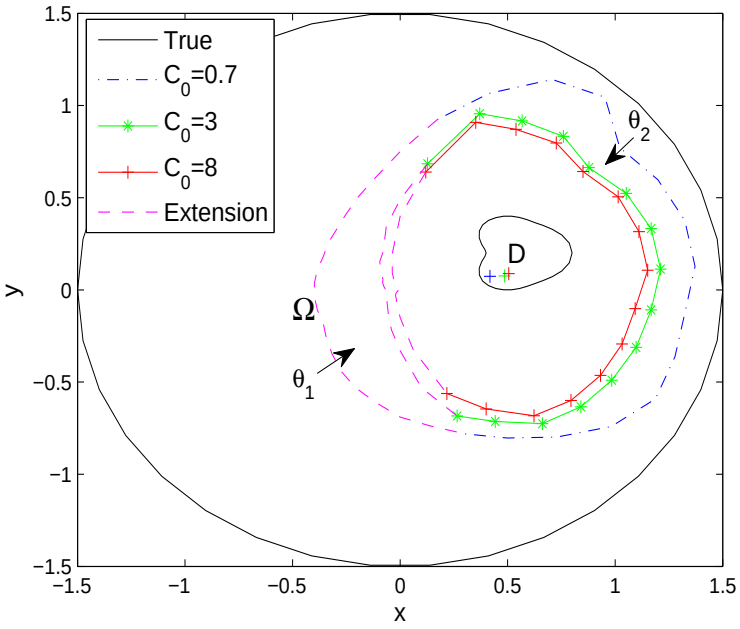

Fig. 5.5. Reconstruction of D for Example 3

6. Conclusions and Discussions

In above figures, it is observed from Figs. 5.3-5.5 that we can get the approximate boundaries of the inclusion D, and numerical results show that our algorithm is effective. In our algorithm, it is important to choose C_θ to simulate the Neumann-to-Dirichlet map. So in the future works, it is expected that more suitable rules for choosing C_θ will be proposed and tested. Although we can minimize the error of the Neumann-to-Dirichlet map using refined meshes, it will increase the error in solving the integral equation (4.2), because we solve (4.2) (which is ill-posed) by

using regular methods. Consequently, a suitable mesh should be chosen to balance the two errors.

Acknowledgments. The second author was supported by the Korea Research Foundation Grant funded by the Korean Government (MOEHRD) under the grant number KRF-2006-214-C00007. The authors thank Prof. R. Potthast (Reeding Univ., UK) and J. Cheng (Fudan Univ., China) for useful discussions.

References

[1] G. Alessandrini and M. Di Cristo, Stable determination of an inclusion by boundary measurements, *SIAM J. Math. Anal.*, **37**:1 (2005), 200-17.

[2] J. Cheng, J.J. Liu and G. Nakamura, The numerical realization of probe method for the inverse scattering problems from the near-field data, *Inverse Probl.*, **21** (2005), 839-55.

[3] Y. Daido, H. Kang and G. Nakamura, A probe method for the inverse boundary value problem of non-stationary heat equations, *Inverse Probl.*, **23** (2007), 1787-800.

[4] Y. Daido, Reconstruction of Inclusion for Inverse Boundary Value Problem of Heat Equation Using Probe Method, Doctral thesis of Hokkaido University, 2007.

[5] P.C. Hansen, Regularization tools: a Matlab package for analysis and solution of discrete ill-posed problems, *Numer. Algorithms*, **6** (1994), 1-35.

[6] A. Friedman,Partial Differential Equations of Parabolic Type, Englewood Cliffs, N.J., 1964.

[7] M. Ikehata, Reconstruction of inclusion from boundary measurements, *J. Inverse and Ill-Posed Problems*, **10** (2002), 37-65.

[8] V. Isakov, K. Kim and G. Nakamura, Reconstruction of an unknown inclusion by thermal imaging, *preprint*, 2007.

[9] V. Isakov, Inverse Problems for Partial Differential Equations (2nd ed.) (Applied Mathematical Sciences vol 127), Springer, New York, 2006.

[10] R. Kress, Linear Integral Equations (2nd ed.), Springer, New York, 1999.

[11] V.D. Kupradze, Three-dimensional Problems of the Mathematical Theory of Elasticity and Thermoelasticity (North-Holland series in Applied Mathematics and Mechanics vol 25), Amsterdam, North-Holland, 1979.

[12] J.L. Lions and M. Magenes, Non-Homogeneous Boundary Value Problems and Applications II, Springer, New York, 1972.

[13] O.A. Ladyženskaja, V.A. Solonnikov and N.N. Uralceva, Linear and Quasi-linear Equations of Parabolic Type (Translations of Mathematical Monographs vol 23), Providence, R.I.: American Mathematical Society, 1968.

[14] E.A. Jr. McIntyre, Boundary integral solutions of the heat equation, *Math. Comput.*, **46** (1986), 71-9.

[15] P.M. Patel, S.K. Lau and D.P. Aldmond, A review of image analysis techniques applied in transient tomographic nondestructive testing, *Nondestructive Testing and Eval.*, **6** (1992), 343-364.

[16] P. Reulet, D. Nortershauser and P. Millan, Inverse method using infrared thermography for surface temperature and heat flux measurements, *Instrumentation in Aerospace Simulation Facilities, ICIASF apos;03. 20th International Congress*, **25** (2003), 118-126.

[17] J. Wloka, Partial Differential Equations (Translated from the German by Thomas C B and Thomas M J), Cambridge University Press, Cambridge, 1987.